frontiers | Frontiers in Virology

TYPE Original Research
PUBLISHED 07 May 2024
DOI 10.3389/fviro.2024.1380030



OPEN ACCESS

EDITED BY
Akio Adachi,
Tokushima University, Japan

REVIEWED BY
Masfique Mehedi,
University of North Dakota, United States
Erguang Li,
Nanjing University, China
Giovanni Piedimonte,
Tulane University, United States

*CORRESPONDENCE
Angela Wahl
awahl@uab.edu
Raymond J. Pickles
raymond_pickles@med.unc.edu

†These authors have contributed equally to this work and share first authorship

RECEIVED 31 January 2024
ACCEPTED 15 April 2024
PUBLISHED 07 May 2024

CITATION
De C, Pickles RJ, Yao W, Liao B, Boone A, Cleary RA, Garcia JV and Wahl A (2024) RSV infection of humanized lung-only mice induces pathological changes resembling severe bronchiolitis and bronchopneumonia. *Front. Virol.* 4:1380030.
doi: 10.3389/fviro.2024.1380030



# RSV infection of humanized lung-only mice induces pathological changes resembling severe bronchiolitis and bronchopneumonia

Chandrav De[1,2,3†], Raymond J. Pickles[4,5*†], Wenbo Yao[1,2,3], Baolin Liao[1,2,3,6], Allison Boone[4,5], Rachel A. Cleary[1,2,3], J. Victor Garcia[1,2,3,7] and Angela Wahl[1,2,3,7*]

[1]International Center for the Advancement of Translational Science, University of North Carolina at Chapel Hill, Chapel Hill, NC, United States, [2]Division of Infectious Diseases, Department of Medicine, University of North Carolina at Chapel Hill, Chapel Hill, NC, United States, [3]Center for AIDS Research, University of North Carolina at Chapel Hill, Chapel Hill, NC, United States, [4]Department of Microbiology and Immunology, University of North Carolina at Chapel Hill, Chapel Hill, NC, United States, [5]Marsico Lung Institute, University of North Carolina at Chapel Hill, Chapel Hill, NC, United States, [6]Department of Infectious Diseases, Guangzhou Eighth People's Hospital, Guangzhou Medical University, Guangzhou, China, [7]Department of Microbiology, University of Alabama at Birmingham, Birmingham, AL, United States

Respiratory syncytial virus (RSV) is a substantial cause of severe lower respiratory tract infections in infants, young children, older adults, and immunocompromised individuals. There is a vital need for effective therapeutics to prevent and/or treat severe RSV infection in these high-risk individuals. The development and pre-clinical testing of candidate RSV therapeutics could be accelerated by their evaluation in animal models that recapitulate bronchiolitis and bronchopneumonia, both hallmark features of severe RSV infection in humans. Previously, we demonstrated that implanted human lung tissue in humanized lung-only mice (LoM) can be infected with RSV, resulting in sustained virus replication. Here we analyzed RSV-associated human lung pathology in the human lung implants of RSV-infected LoM. RSV-infected epithelial cells lining the airway and the alveolar regions of human lung implants result in hallmark histological features of RSV bronchiolitis and bronchopneumonia, including distal airway and alveolar lumens clogged with (1) sloughed and necrotic RSV-infected epithelial cells, (2) neutrophil-containing inflammatory infiltrates, and (3) MUC5B-dominated mucus secretions. We also show that treatment of LoM with a small molecule antiviral (ribavirin) or a neutralizing antibody (palivizumab) significantly suppressed and/or prevented RSV infection *in vivo*. Our data together show that RSV infection of human lung implants *in vivo* exhibits appropriate cellular tropism and results in the hallmark pathological characteristics of severe bronchiolitis and bronchopneumonia in humans. They also offer proof-of-principle of the utility of this model to evaluate novel approaches for the prevention/treatment of RSV infection.

KEYWORDS

**respiratory syncytial virus, RSV, humanized mice, LoM, human lung pathology, therapeutics**

# Introduction

Most acute lower respiratory tract infections in infants and young children are attributed to infection by respiratory syncytial virus (RSV). Globally, RSV infection causes over three million hospital admissions and 100,000 deaths in children under 5 years of age annually (1–3). RSV infection also leads to considerable morbidity and mortality in the elderly, transplant patients, and other immunosuppressed individuals (4–7). Since the onset of the COVID-19 pandemic, there have been multiple unprecedented surges in RSV infections, resulting in a substantial increase in severe RSV cases and hospitalizations among children and older adults (8, 9).

Recently, two RSV vaccines targeting the RSV prefusion F protein have been approved for clinical use to prevent RSV infection of infants and/or adults aged 60 and older. However, uptake of the RSV vaccine has been low, with less than 20% of adults age 60 and older vaccinated in the US (10). Currently, only three medications are approved to prevent/treat RSV infection. Palivizumab and long-acting nirsevimab are monoclonal antibodies that are administered prophylactically to high-risk children to prevent severe respiratory disease. In addition to supportive care, aerosolized or oral ribavirin, a nucleoside analog, is used to treat severe lower respiratory tract infections in hospitalized pediatric patients (11–14). Candidate RSV therapeutics in development include agents that target virus entry (RSV F protein inhibitors) or virus replication (polymerase inhibitors) (15).

The development and pre-clinical testing of candidate RSV therapeutics could be accelerated by their evaluation in animal models that recapitulate bronchiolitis and bronchopneumonia, both hallmark features of severe RSV infection of humans. The pathological features of severe RSV infection of humans are characterized by infection and inflammation of the bronchioles and alveolar regions of the lung (16). RSV bronchiolitis caused by infection and inflammation of the narrow-diameter bronchiolar airways leads to occlusion of the airway lumen with sloughed and necrotic epithelial cells, neutrophil-rich inflammatory infiltrates, and variable quantities of mucous secretions (17). In the alveolar regions, RSV infection results in alveolar spaces containing sloughed epithelial cells, viral-antigen-rich cellular debris, and inflammatory infiltrates (16). As a consequence, prolonged obstruction of the bronchiolar airways and alveolar spaces by shed cells and inflammatory infiltrates, especially in human infants, restricts normal airflow, leading to alveolar gas trapping and alveolar collapse manifesting as more severe symptoms of respiratory disease.

Humanized lung-only mice or LoM possess subcutaneous human lung implants that contain human endothelial, epithelial, and fibroblast cells that form human lung structures, including small-diameter respiratory airways (18–20). Previously, we demonstrated that RSV efficiently replicates in human lung implants (18, 20). Our aim here was to evaluate the histopathology of RSV infection in human lung implants to determine if RSV infection of LoM recapitulates the features of severe RSV lung disease in humans and to demonstrate the utility of this model for evaluating treatment interventions.

# Materials and methods

## Experimental design

To analyze RSV infection, LoM human lung implants were injected with virus expressing GFP or luciferase reporter genes, and the virus-infected cells were analyzed by IVIS imaging (luciferase activity), flow cytometry (GFP), and/or histology (RSV antigen staining) (18, 20). Studies in LoM were carried out according to the University of North Carolina-Chapel Hill Institutional Use and Care Committee protocols #17-288 and 20-235 and in observance of the National Institutes of Health Guide for the Care and Use of Laboratory Animals. These studies use LoM human lung implants previously analyzed for RSV infection kinetics (20) to evaluate the histological and pathological consequences of RSV infection of human lung implants (Figures 1–3; Supplementary Figures S1-S3).

## Generation of humanized mice

LoM (Supplementary Table S1) were generated as described previously (18–20). Briefly, LoM were constructed by the subcutaneous implantation of a piece of human lung tissue (Advanced Bioscience Resources) into two regions (upper and lower) of the back of male and female NOD.Cg-Prkdcscid ll2rgtm1Wjl/SzJ mice (NSG mice; The Jackson Laboratory) (18–20). At 10 weeks post-implantation, a time when the lung implants are palpable under the skin, LoM with one or two human lung implants were used for experimentation. The mice were maintained by the Division of Comparative Medicine at the University of North Carolina—Chapel Hill using specific pathogen-free conditions.

## Viruses and *in vivo* analysis of infection

Stocks of RSV strain A2 expressing green fluorescent protein (GFP) (21) or firefly luciferase (Luc) reporter genes were obtained from Viratree. LoM were anesthetized, and then RSV A2-GFP or RSV A2-Luc was injected ($2.5 \times 10^5$ $TCID_{50}$, 100 µL volume) into each human lung implant (20). At necropsy, human lung implants were collected for analysis by flow cytometry, qRT-PCR, and/or histology as previously described (18, 20). RSV infection in LoM exposed to RSV-A2 GFP was evaluated by measuring GFP-expressing cells using flow cytometry (20). Briefly, human lung implants were minced, enzymatically digested, and passed through a cell strainer to create a single-cell suspension. The cells were washed, fixed with 2% paraformaldehyde (PFA), and analyzed on a BD LSRFortessa instrument with BD FACSDiva (version 6.1.3) and FlowJo (version 10.6.2) software. RSV infection in LoM exposed to RSV A2-Luc was evaluated by measuring the luciferase activity *in situ* with an *in vivo* imaging system (IVIS) as previously described (20). *In vivo* imaging was performed with a CCD camera (Xenogen IVIS-Lumina, Perkin Elmer, MA, USA) as previously described (20). The mice were administered D-Luciferin (15 mg $kg^{-1}$, intraperitoneal injection) 5 min prior to imaging. The mice were anesthetized with isoflurane (2% in oxygen), and bioluminescence

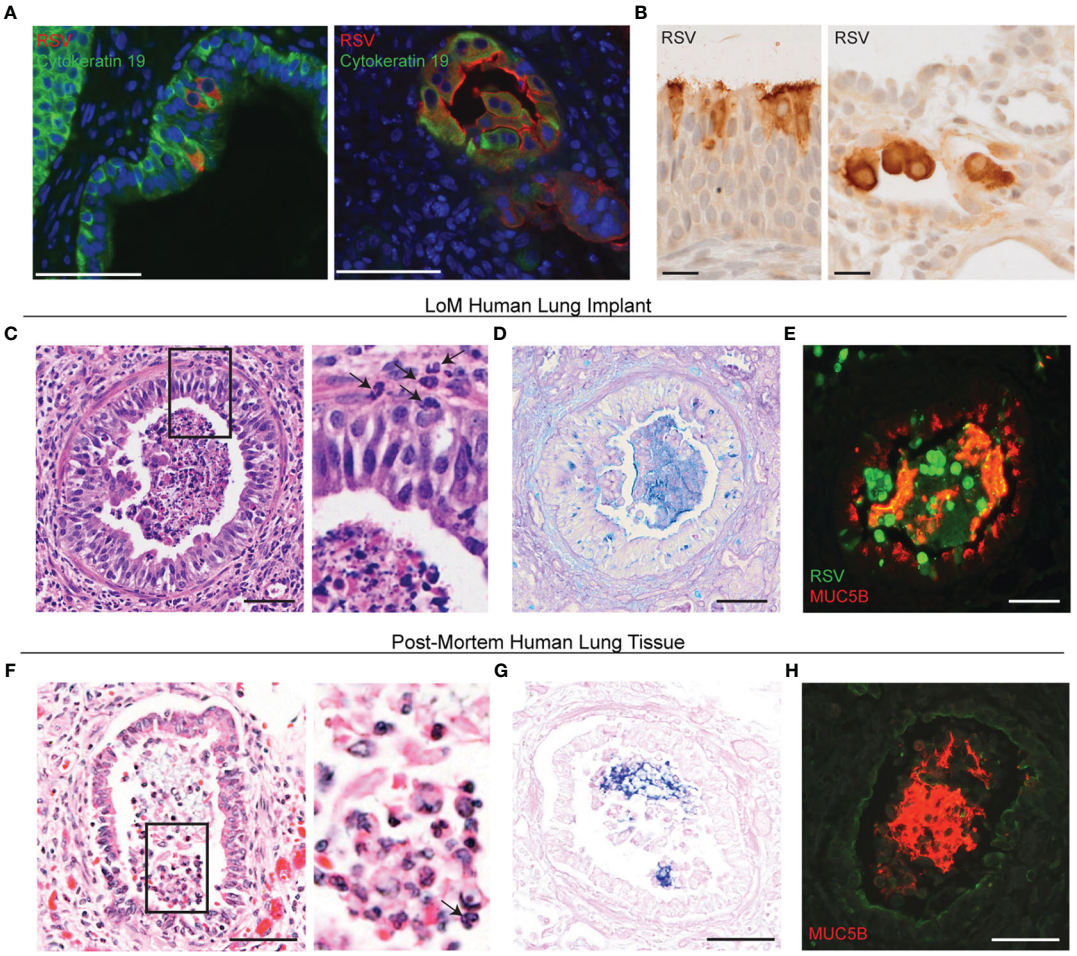


FIGURE 1
RSV infection induces bronchiolitis in LoM human lung implants. **(A)** Immunofluorescence staining for RSV (red) and cytokeratin 19 (green) in the human lung implants of RSV-infected LoM (*n* = 5 implants analyzed). Shown are images from two RSV-Luc-infected LoM at 21 days post-infection. The nuclei are blue. Scale bars, 68 um. **(B)** Immunohistochemical staining for RSV antigen (dark brown) in the human lung implants of an RSV-Luc-infected LoM at 4 days post-infection, demonstrating RSV infection of ciliated columnar epithelial cells and cuboidal alveolar epithelial cells. Scale bars, 20 um. **(C)** H&E staining (*n* = 12 implants analyzed), **(D)** Alcian blue periodic acid-Schiff (AB-PAS) staining for mucus secretions (blue, *n* = 6 implants analyzed), and **(E)** immunofluorescence co-staining (*n* = 4 implants analyzed) for RSV-infected cells (green) and MUC5B (red) in the airway of an RSV-infected LoM human lung implant. Images shown from RSV-GFP-infected LoM at 7 days post-RSV infection. **(F)** H&E staining, **(G)** AB-PAS staining for mucus secretions (blue), and **(H)** immunofluorescence staining for MUC5B (red) in post-mortem lung tissue obtained from an RSV-infected infant (*n* = 1 analyzed). Scale bars, 50 um. Note: Surface of airway epithelium counterstained for MUC1 (green). Arrows note neutrophils in **(C, F)**.

images were acquired for 3 min (f/stop = 1.2, binning = 4). Photon emissions within constant regions of interest (ROI) were measured as radiance in $p\,s^{-1}\,cm^{-2}\,sr^{-1}$ and were presented as total flux (photons/s). Background luminescence in LoM human lung implants was determined prior to RSV exposure.

## Palivizumab and ribavirin treatment

To evaluate the effect of palivizumab on RSV infection in human lung implants, LoM received one dose of palivizumab (15 or 30 mg/kg) via intramuscular injection either one day prior to or one day after exposure to RSV A2-GFP. At 4 days post-RSV exposure, LoM were necropsied, and the number of GFP-expressing cells in the human lung implants of palivizumab-treated LoM and untreated controls was measured by flow cytometry. To evaluate the effect of ribavirin on RSV infection in human lung implants, LoM were administered ribavirin (40 mg/kg) daily via intraperitoneal injection starting 1 day prior to or 1 day after exposure to RSV A2-Luc. The untreated RSV-infected LoM served as controls. The RSV luciferase activity was measured in the human lung implants of LoM by IVIS imaging prior to RSV exposure and at 7 days post-RSV exposure.

## qRT-PCR analysis

Human lung implants were minced and then homogenized further with Minilys Tissue Homogenizer (Bertin Instruments). The samples were then centrifuged (1,600 RPM, 4°C, 5 min), and 200 µL of

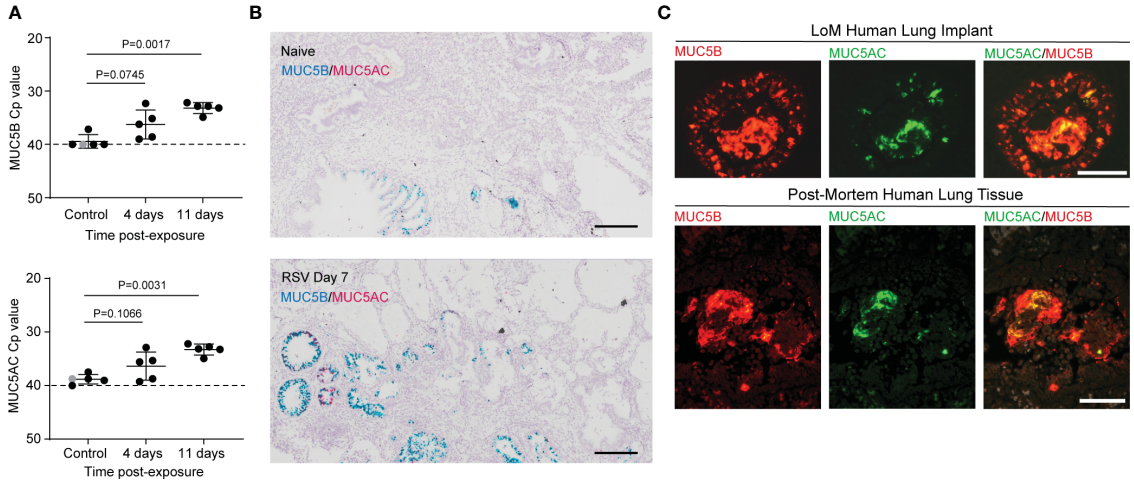


FIGURE 2
RSV infection induces mucin production in human lung implants. **(A)** Quantitation by qRT-PCR of *MUC5B* (top) and *MUC5AC* (bottom) mRNA expression in homogenates of human lung implants collected from control LoM (naïve, *n* = 1, shown in gray or 2 h post-RSV exposure, *n* = 4, shown in black) and RSV-infected LoM at 4 and 11 days post-exposure (*n* = 5 implants/time point). Crossing point (Cp): the cycle at which the sample's fluorescence signal exceeds background fluorescence. Horizontal and vertical lines represent the mean and standard deviation, respectively. Statistical significance was determined with a two-tailed Kruskal–Wallis test, and *P*-values were adjusted for multiple testing using the Benjamini, Krieger, and Yekutieli false-discovery rate method. **(B)** *In situ* RNA hybridization for *MUC5B* (blue) and *MUC5AC* (pink) mRNA in a naïve LoM human lung implant (top panel, *n* = 4 analyzed) and an RSV-infected LoM human lung implant at 7 days post-exposure (bottom panel, *n* = 4 analyzed). Scale bars, 200 uM. **(C)** Immunofluorescence staining for MUC5B (red) and MUC5AC (green) antigen in an RSV-infected LoM human lung implant at 7 days post-exposure (top panels, *n* = 4 analyzed) and in post-mortem lung tissue obtained from an RSV-infected infant (bottom panels, *n* = 1 analyzed). Scale bars, 50 uM.

homogenate supernatant was combined with 600 µL of Trizol. Subsequently, the samples were vortexed, and RNA was extracted using the Direct-zol RNA Miniprep kit (Zymo Research) according to the manufacturer's instructions. The RNA concentrations were determined (NanoDrop One, Thermo Fisher), and 500 ng RNA was used to generate cDNA (iScript Reverse Transcription Supermix for qRT-PCR, BioRad) which was diluted 20-fold in Tris-EDTA buffer, pH 8.0 (Amresco). qRT-PCR was performed using SsOAdvanced Universal Probes or Advanced Universal SYBR Green Supermix (depending on the primers) according to the manufacturer's instructions. The relative expression of *MUC5B* and *MUC5AC* was quantified using Quant6 Studio Flex software based on the cycle at which the sample's fluorescence signal exceeds background fluorescence (the "crossing point" or $C_p$). Target expression inversely correlated with $C_p$ values.

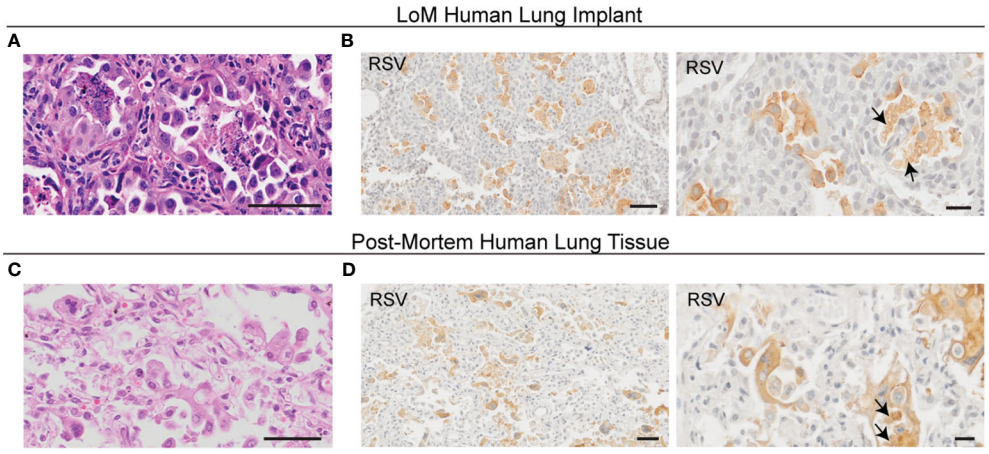


FIGURE 3
RSV infection alters the human epithelial cell morphology in LoM. **(A)** H&E staining (*n* = 12 implants analyzed, scale bars, 50 um) and **(B)** IHC staining for RSV antigen (brown; *n* = 4 implants analyzed; left scale bar, 50 um; right scale bar, 20 um) in alveolar regions of an RSV-infected LoM human lung implant. Images shown from RSV-infected LoM at 4 days post-RSV infection. **(C)** H&E staining (scale bars, 50 um) and **(D)** IHC staining for RSV antigen (brown; left scale bar, 50 um; right scale bar, 20 um) in alveolar regions in post-mortem lung tissue obtained from an infant who died from RSV pneumonia (*n* = 3 analyzed). Arrows note necrotic cell debris positive for RSV in the airspace lumen in **(B, D)**.

## Histological staining

Histological sections of human lung implants harvested from LoM were fixed in 4% PFA or 10% formalin, embedded in paraffin, and 5-µm-sections were cut as previously described (18–20). De-identified paraffin-embedded post-mortem lung tissues obtained from infants with established RSV infections were kindly provided by Drs. Barney Graham and Alan Proria, and 5-µm histological sections were used. Standard histological staining, including H&E and Alcian-blue periodic acid-Schiff (AB-PAS) staining, was performed on naive control and RSV-infected LoM human lung implants and on post-mortem human lung tissue by the UNC Pathology Services Core. Immunohistochemical (IHC) and immunofluorescence (IF) staining were performed as previously described (18–20). Briefly, tissue sections were deparaffinized with xylene and an ethanol gradient. For IHC, primary antibodies were added to tissue sections after antigen retrieval (30 min, 95°C, 1X DIVA Decloaker, Biocare Medical) and blocking of non-specific Ig-binding sites (20 min, RT, Background Sniper, Biocare Medical). A primary goat antibody directed against RSV nucleoprotein was used to detect RSV-infected cells (Meridian Biosciences or Abcam). Tissue sections were also stained with a goat IgG isotype control antibody (Supplementary Figure S1). Tissue sections were developed using ImmPRESS® HRP Horse Anti-Goat IgG peroxidase Polymer Detection Kit (Vector Laboratories) following the blocking of endogenous peroxidase activity (10 min, RT, 1.5% hydrogen peroxide in TBST), and then counterstained with hematoxylin. For IF staining, following antigen retrieval and blocking of Ig-binding sites as described above, tissue sections were probed with an antibody directed against RSV (goat polyclonal, Meridian Biosciences or Abcam), human cytokeratin 19 (clone EPR1579Y, Abcam), MUC5AC (clone 45M1, Thermo Fisher), and/or MUC5B (clone H300, Santa Cruz Biotechnology). Following primary antibody incubation, the tissue sections were incubated with fluorescent secondary antibodies (Alexa fluor, Molecular Probes, Thermo Fisher Scientific) and stained with DAPI. The tissue sections were imaged on a Nikon Eclipse Ci microscope with a Nikon Digital Sight DS-Fi2 camera using Nikon Elements BR software (version 4.30.01) or on an Olympus VS120 virtual slide scanning system with an Allied Vision Pike 5 CCD progressive scan camera using OlyVia software (version 2.9). The brightness, contrast, and white balance on whole images were adjusted using Adobe Photoshop (CS6).

RNA *in situ* hybridization for *MUC5AC* and *MUC5B* was performed on paraffin-embedded sections using RNAscope Advanced Cell Diagnostics (ACD) 2.5HD Duplex Assay (322435, ACD) according to the manufacturer's instructions. The tissue sections were deparaffinized with xylene (twice for 5 min) and 100% ethanol (twice for 1 min) and incubated with hydrogen peroxide for 10 min. Target retrieval was performed in boiling water for 15 min, followed by incubation with Protease Plus (322330, ACD) at 40°C for 15 min. The tissue sections were hybridized with custom probes for *MUC5AC* and *MUC5B* at 40° C for 2 h using a HybEZ oven (241000, ACD), and the signals were amplified according to the manufacturer's instructions. The slides were scanned and digitized using an Olympus VS200 light and fluorescent microscope with ×40 0.95 N.A. Ubiquitin C (UBC) and bacterial DapB gene probes were used for positive and negative controls, respectively.

## Statistical analysis

Group sizes are indicated in the figure legends and in Supplementary Table S1. No statistical methods were used to determine sample sizes, no randomization methods were used to allocate mice to experimental groups, and the investigators were not blinded by the experimental group to ensure that appropriate reagents were used. No data points were excluded from the analysis. Statistical tests were performed in GraphPad Prism (version 6). The statistical tests performed are indicated in the figure legends. *P*-values were adjusted for multiple testing as indicated in the figure legends. For all statistical comparisons, $P < 0.05$ was considered significant.

# Results

## RSV infects human epithelial cells lining the lower respiratory tract

LoM were constructed by subcutaneously implanting human lung tissue into the back of immunodeficient mice. The direct injection of RSV into the human lung implants of LoM results in sustained virus replication for over 10 weeks (18, 20). RSV infected human epithelial cells lining both the airways and alveolar spaces (Figure 1A). Based on morphological criteria, this includes ciliated columnar epithelial cells of the airway epithelium and simple cuboidal epithelial cells in the alveolar regions of human lung implants (Figures 1A, B). These results recapitulate the tropism of RSV demonstrated in the airways during natural RSV infection of the human lung (16, 22). It should be noted that this specific tropism differentiates the cellular targets of RSV infection from those of other viruses that target the lungs such as MERS-CoV, HCMV, and Zika virus (18, 19).

## RSV infection in human lung implants reproduce the hallmark histological features of RSV infection of the distal airways of humans

We used LoM human lung implants previously analyzed for RSV replication (20) to compare the histological consequences of RSV infection of bronchiolar airways in human lung implants to previously reported consequences with severe, untreated RSV infections in humans (22). RSV infection of human lung implants with RSV A2-GFP resulted in the accumulation of sloughed GFP-positive epithelial cells, neutrophil-containing inflammatory infiltrates, and mucus secretions in the distal airway lumens (Figures 1C–E) (17, 22). Importantly, these histological findings were remarkably similar to those in the distal airways of humans with natural RSV infection as demonstrated by distal airway lumens

containing sloughed and necrotic epithelial cells, neutrophil inflammatory infiltrates, and variable quantities of mucus secretions (22). Peri-airway thickening, a histopathological feature of human RSV infection (23), was observed in the human lung implants of RSV-infected LoM (Supplementary Figure S2). In RSV-infected LoM human lung implants (Figure 1C) and post-mortem lung tissue obtained from a pediatric patient with severe RSV bronchiolitis (Figure 1F, Supplementary Figure S3A), neutrophils were seen infiltrating the airway lumen. The cellular debris in the airway lumens also showed patchy Alcian Blue Periodic Acid-Schiff (AB-PAS) staining indicative of highly glycosylated mucins in RSV-infected LoM human lung implants (Figure 1D) and pediatric post-mortem lung tissue (Figure 1G). As MUC5B has been recently shown to be the predominant gel-forming mucin secreted from the distal airways of humans under baseline conditions (24), we confirmed that MUC5B was the major secreted gel-forming mucin present in the AB-PAS-positive material accumulating in the distal airway lumens in both human lung implants (Figure 1E, Supplementary Figure S3B) and lung tissues during natural RSV infection (Figure 1H). Therefore, these data confirm the utility of human lung implants as *in vivo* models which reproduce the hallmark histological features of RSV infection of the distal airways of humans.

## The secreted mucin MUC5B is the predominant gel-forming mucin formed during RSV infection of distal airways

The human airway epithelium can induce the expression and secretion of two major gel-forming mucins, MUC5B and MUC5AC. Studies in humans and mice have suggested that MUC5B/Muc5b is a beneficial secreted mucin contributing to lung health, while MUC5AC/Muc5ac is a pathologic mucin attributed to pathological states (25). For these reasons, most mouse models of RSV infection have previously emphasized the extent of Muc5ac production as a marker of increased lung disease as a consequence of RSV infection. To confirm our histological findings that MUC5B is the predominant secreted mucin present in RSV-infected human lung implants, we measured the mRNA levels of the two major airway gel-forming mucins, MUC5B and MUC5AC, in control LoM and RSV-infected LoM at days 4 and 11 post-RSV exposure by qRT-PCR. We previously confirmed RSV infection of LoM human lung implants by qRT-PCR and virus tittering (20). In whole-tissue homogenates, the mRNA levels of both MUC5B ($P = 0.0017$) and MUC5AC ($P = 0.0031$) were higher at day 11 post-exposure compared to those of the controls (Figure 2A). However, *in situ* RNA hybridization for MUC5B and MUC5AC mRNA demonstrated that MUC5B mRNA was the predominant mucin gene expressed in histological sections of RSV-infected human lung implants (Figure 2B). The predominance of MUC5B protein in the mucus secretions was confirmed using antibodies specific to MUC5B and MUC5AC (Figure 2C). In the airway lumen, sloughed RSV-infected cells were in close association with the MUC5B-rich mucus secretions (Figure 2C). The observations that RSV infection of human lung implants resulted in the accumulation of sloughed, virus-infected epithelial cells and MUC5B-rich mucus secretions in the airway lumens were mirrored in the histological sections of lungs obtained from a pediatric case of severe RSV bronchiolitis (Figures 1F–H, 2C).

## RSV infects the alveolar regions of human lung implants causing bronchopneumonia

Severe RSV infections, especially those in immunocompromised individuals, often result in bronchopneumonia with infection and inflammation in lung alveolar regions (5–7). RSV-infected human lung implants in LoM revealed a robust RSV infection of the alveolar regions with substantial morphologic consequences (Figures 3A, B). The immunohistochemistry results showed abundant pleomorphic epithelial cells containing RSV antigen sloughing from the basal lamina into the lumens of the alveolus (Figure 3B). RSV antigen was also abundant in other surrounding material, likely representing the remnants of RSV-infected cells after necrosis (Figure 3B). These data indicate that the epithelial cells of the alveolar regions of human lung implants are highly susceptible to RSV infection, resulting in significant morphological changes to the alveolar epithelial cells. Pleomorphic RSV antigen-positive epithelial cells and cell remnants were also observed in the alveolar regions of humans experiencing severe RSV bronchopneumonia (Figures 3C, D) as described previously (16).

## Palivizumab and ribavirin prevent and/or control RSV infection in LoM

To demonstrate the utility of LoM to test potential therapeutics directed at reducing RSV infection, we evaluated the ability of two approved anti-RSV therapeutics, the neutralizing antibody palivizumab and the nucleoside inhibitor ribavirin, to limit RSV infection in LoM. LoM were administered palivizumab once either 24 h prior to or 24 h post-RSV A2-GFP exposure (Figure 4A), and the number of GFP+ cells in human lung implants was measured at day 4 post-exposure by flow cytometry (Figure 4B). No GFP+ cells were detected in LoM administered 30 mg/kg palivizumab prior to RSV exposure (Figure 4B). The number of GFP+ cells in the lung implants of LoM administered 15 mg/kg palivizumab prior to RSV exposure was over 7-fold lower ($170.9 \pm 126.8$ GFP+ cells/$10^6$ live cells, $P = 0.0129$) compared to the untreated control animals ($1{,}240.3 \pm 260.6$ GFP+ cells/$10^6$ live cells) (Figure 4B). The numbers of GFP+ cells in the human lung implants of LoM treated with 30 mg/kg palivizumab 24 h post-RSV exposure were 20-fold lower ($60.8 \pm 4$ GFP+ cells/$10^6$ live cells, $P = 0.0210$) compared to the untreated control LoM (Figure 4B).

We also evaluated the effect of ribavirin on RSV replication when administered systemically pre- or post-RSV exposure. LoM were administered ribavirin daily (40 mg/kg/day) initiated 24 h before or after RSV-Luc exposure (Figure 4C). When compared to untreated control LoM ($2.6 \times 10^8 \pm 6.8 \times 10^7$ s.e.m. radiance) at 7 days post-RSV exposure, RSV-luciferase bioluminescence was 90-fold lower in the human lung implants of LoM administered ribavirin before exposure ($2.9 \times 10^6 \pm 1.8 \times 10^6$ s.e.m. radiance, $P$

= 0.0006) and 20-fold lower in the human lung implants of LoM administered ribavirin after exposure ($1.5 \times 10^7 \pm 5.8 \times 10^6$ s.e.m. radiance, $P = 0.0334$) (Figure 4D). Immunohistochemical staining for RSV antigen was used to confirm an abundance of RSV-infected cells throughout the human lung implants of untreated, RSV-exposed LoM (Figure 4E). In contrast, the RSV-infected cells were less abundant in LoM administered ribavirin post-RSV exposure. Notably, RSV-infected cells were not readily detected in the human lung implants of LoM administered ribavirin prior to RSV exposure (Figure 4E). Consistent with a lack of infection, no overt changes

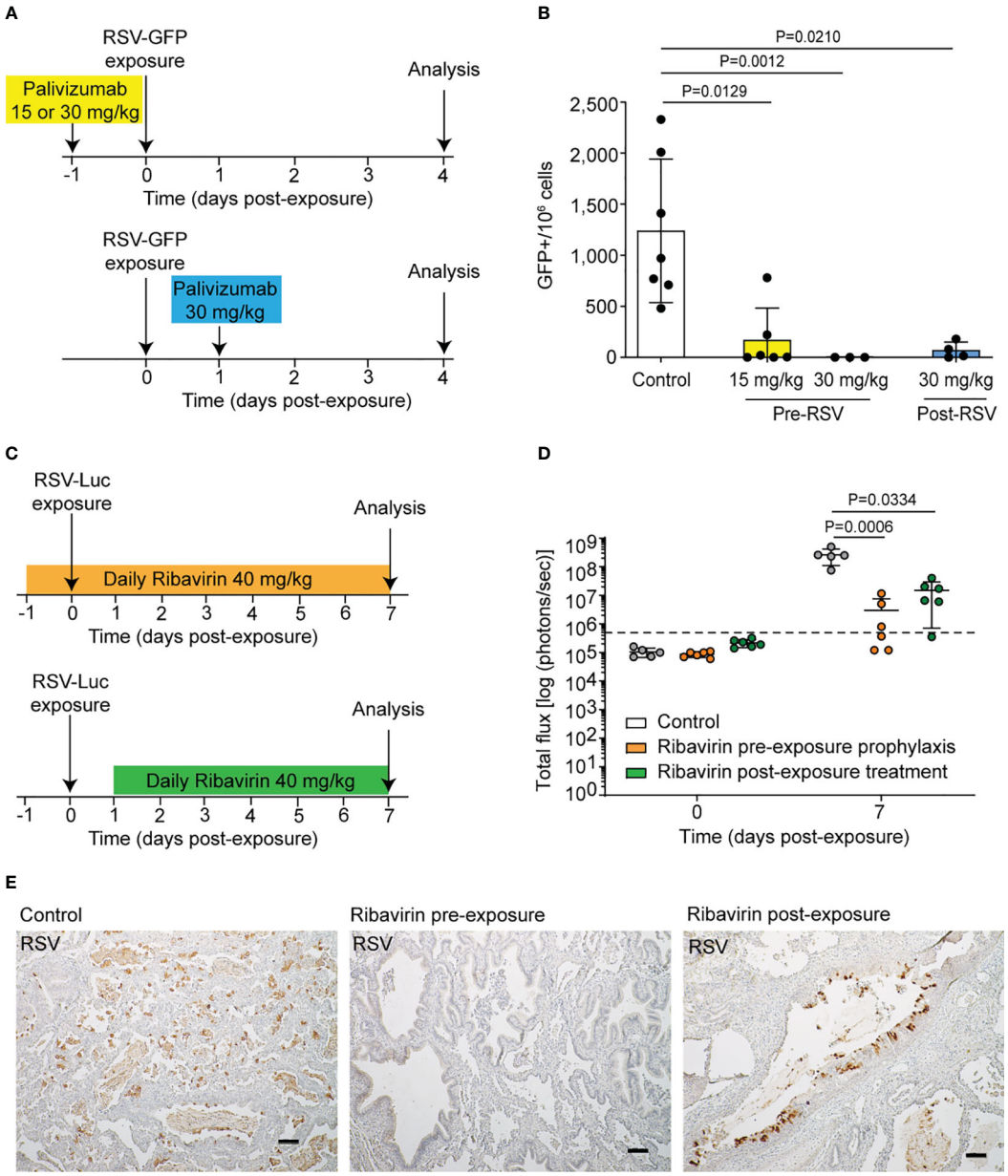


FIGURE 4
LoM are a robust platform for the *in vivo* evaluation of RSV preventative and therapeutic approaches. **(A)** LoM were administered a single intramuscular dose of palivizumab 24 h prior to RSV A2-GFP exposure (15 or 30 mg/kg) or 24 h post-RSV A2-GFP exposure (30 mg/kg). Untreated RSV-GFP-infected LoM served as a control. **(B)** GFP+ cells in human lung implants 4 days post-RSV exposure in untreated LoM ($n$ = 7 implants) and LoM administered palivizumab pre-RSV exposure (15 mg/kg, $n$ = 6 implants and 30 mg/kg, $n$ = 3 implants) or post-RSV exposure ($n$ = 4 implants). **(C)** Ribavirin was administered to mice once daily (40 mg/kg, intraperitoneal) starting 24 h before or after RSV exposure. Untreated RSV-Luc-infected LoM served as a control. **(D)** Bioluminescence signal [radiance (p $s^{-1}$ $cm^{-2}$ $sr^{-1}$) represented as total flux] in human lung implants just prior to RSV exposure and at 7 days post-RSV exposure in untreated LoM (white bars, $n$ = 5 implants) and LoM administered ribavirin treatment initiated pre-RSV exposure (orange bars, $n$ = 6 implants) or post-RSV exposure (green bars, $n$ = 6 implants). The mean (horizontal line) and standard deviation (vertical line) are shown. Background luminescence measured pre-exposure is denoted by the dashed line. **(E)** Immunohistochemical staining for RSV antigen (brown) in human lung implants 7 days post-RSV exposure in untreated LoM (left panel) and LoM administered ribavirin treatment initiated pre-RSV exposure (middle panel) or post-RSV exposure (right panel). Scale bars, 100 um; $n$ = 3 implants analyzed. **(B, D)** Data are shown as mean ± SD. Results from the treated groups were compared to untreated controls using a two-tailed Kruskal–Wallis test, and $P$-values were adjusted for multiple testing using the Benjamini, Krieger, and Yekutieli false-discovery rate method.

were noted in tissue structures. These results altogether demonstrate that the FDA-approved drugs palivizumab and ribavirin dramatically reduce RSV replication in LoM.

## Discussion

*In vivo* models that recapitulate the pathophysiology of RSV infection in the human lung are critical for the continued development and implementation of novel therapeutics to prevent and/or control RSV infection. Three-dimensional organoid models of human fetal lungs have been used to model *in utero* RSV infection of first-trimester lungs. Interestingly, RSV infected fetal mesodermal and mesenchymal cells more frequently than fetal lung epithelial cells, indicating gestational differences in the cell types targeted by RSV infection in the lung (26). Previously, we demonstrated that the human epithelial cells present in the human lung implants of LoM are susceptible to RSV infection and that virus replication is maintained over time in the absence of an autologous adaptive human immune response (18, 20). Here we demonstrate that RSV infection of LoM faithfully recapitulates key aspects of RSV pathology in humans. Specifically, using LoM, we recapitulated the hallmark characteristics of RSV infection documented in the airways and lungs of infants with severe disease, most notably robust RSV infection of epithelial cells resulting in the accumulation of sloughed and necrotic epithelial cells, neutrophil-rich inflammatory infiltrates, and mucus secretions in the distal airway lumens as well as peri-bronchial thickening (17, 20, 22, 23). These outcomes together recapitulated the hallmark characteristics of severe RSV bronchiolitis and bronchopneumonia in humans. Furthermore, treatment with antivirals or neutralizing antibodies efficiently suppressed and/or prevented RSV infection in human lung implants, offering proof-of-principle of the utility of this model to evaluate novel approaches *in vivo* for their ability to prevent and/or treat severe RSV infection.

The accumulation of muco-cellular material in the distal airway lumens of LoM is remarkably consistent with the pathologic findings described in the bronchiolar airways of infants naturally infected by RSV (17, 22). Previous studies in mice have shown RSV inoculation results in increased expression of mucin genes in the lower airways and increased AB-PAS-positive material in the airway lumens. However, evidence for RSV infection in the mouse airway epithelium resulting in the accumulation of sloughed, virus-infected epithelial cells, and neutrophil-rich inflammatory infiltrates in the airway lumens is lacking (27–29). Furthermore, studies in mice have largely focused on the upregulation of the gel-forming secreted mucin, Muc5ac, during RSV infection (29, 30). In contrast, our studies comparing the consequences of infection in human lung implants to those in previously reported histological studies of lungs from RSV-infected individuals reveal RSV infection of the airway epithelial cells resulting in distal airway lumens becoming clogged by sloughed and necrotic epithelial cells, neutrophil-rich inflammatory infiltrates, and MUC5B-rich mucus secretions. We also observed increased neutrophil infiltrates into RSV-infected human lung implants as previously described (20). While the infiltrating neutrophils in RSV-infected LoM are mouse in origin and not human neutrophils, our results are consistent with the abundance of neutrophils present in bronchoalveolar lavages from RSV-infected children and post-mortem histopathologic analyses of fatal RSV-related cases (22, 31–33).

RSV infection results in a characteristic pleomorphic morphology of columnar airway epithelial cells *in vitro* and *in vivo* (34), which is not observed by RSV infection of commonly investigated laboratory cell lines. Indeed it was previously demonstrated that the pleomorphic morphology of RSV-infected columnar epithelial cells was driven by the RSV non-structural Protein 2 (NS2) (34). It was speculated that NS2 may prolong the survival of shed RSV-infected cells by suppressing anoikis (cell-detachment-induced apoptosis), resulting in the accumulation of shed but intact RSV-infected cells in the lumen. It is possible that this subversion of anoikis is responsible for shed epithelial cells eventually becoming necrotic in the airway lumen, thus providing a highly inflammatory environment in the airway lumen. The accumulation of inflamed and necrotic muco-cellular materials in the distal airways of humans is an important contributor to the obstruction of normal airflow in RSV-infected patients and a well-defined clinical feature of severe RSV bronchiolitis (17, 22). Therefore, it represents an important target for the development of novel therapeutic interventions that can be readily evaluated in LoM.

RSV infection has been previously shown to injure the airway epithelium by disrupting cell–cell contacts (35). *In vitro* studies have also shown that RSV infection delays the repair of the airway epithelium by inducing remodeling of the actin cytoskeleton, stress fiber formation, and the development of focal adhesions, impeding epithelial cell migration (36). In the future, it would be interesting to evaluate the ability of RSV to attenuate epithelial cell migration, a step in wound repair, promote stress fiber formation, and mediate the assembly of large focal adhesions in human lung implants of LoM which sustain virus replication and BLT-Lung mice which have a systemic autologous human immune system that controls virus replication (18, 20).

We also show that two FDA-approved drugs, palivizumab and ribavirin, reduced RSV replication in LoM when administered prior to or after RSV exposure, validating LoM as a platform for testing the efficacy of systemically administered antivirals and biologics to prevent and/or treat RSV infection. A limitation of LoM is the inability to deliver therapeutics to the lung by aerosol delivery, although direct instillation of therapeutics into the lumen of the airways and alveolar regions is possible in addition to the systemic delivery of reagents to LoM. LoM are also devoid of upper airway regions and larger lower airway structures (e.g., nasopharynx, larynx, and trachea) which are likely airway regions important in initiating RSV infection in humans. However, RSV infections limited to the upper respiratory tract are usually mild, while more severe infections are indicative of infection of the bronchiolar airways and the alveolar lung regions. Previously, we demonstrated that LoM support the replication of other human viral and bacterial pathogens that target the lung, including SARS-CoV, SARS-CoV-2, MERS-CoV, HCMV, zika virus, and mycobacteria, without requiring adaptation of the specific pathogens to animal models (18, 19). As RSV circulates in the human population simultaneously with other respiratory viruses

including SARS-CoV-2, influenza viruses, human parainfluenza viruses, human metapneumoviruses, and rhinoviruses, studies that will explore the impact of multiple simultaneous virus infections in LoM are warranted (37–39). Bacterial co-infection is also reported in children with severe RSV bronchiolitis, and LoM could be used as an investigational platform to evaluate these viral and bacterial poly-infections.

In summary, our results demonstrate that (1) RSV infection of LoM results in histopathology characteristic of severe RSV infection in humans including bronchiolitis and bronchopneumonia (2), RSV infection of LoM recapitulates the obstruction of distal airways by sloughed and necrotic epithelial cells, neutrophil-rich inflammatory infiltrates, and mucus secretions, and (3) approved therapeutic interventions against RSV efficiently prevent and/or suppress RSV infection in LoM, providing proof-of-principle that this *in vivo* model provides a robust platform for the evaluation of RSV preventative and therapeutic approaches.

## Data availability statement

The original contributions presented in the study are included in the article/Supplementary Material. Further inquiries can be directed to the corresponding authors.

## Ethics statement

Ethical approval was not required for the studies involving humans because this study used retrospective de-identified human lung sections. The studies were conducted in accordance with the local legislation and institutional requirements. The human samples used in this study were gifted from another research group. Written informed consent to participate in this study was not required from the participants or the participants' legal guardians/next of kin in accordance with the national legislation and the institutional requirements. The animal study was approved by University of North Carolina at Chapel Hill Institutional Animal Care and Use Committee. The study was conducted in accordance with the local legislation and institutional requirements.

## Author contributions

CD: Conceptualization, Methodology, Project administration, Visualization, Writing – original draft, Writing – review & editing, Formal analysis, Investigation. RP: Conceptualization, Formal analysis, Investigation, Project administration, Visualization, Writing – original draft, Writing – review & editing, Funding acquisition, Resources, Supervision. WY: Investigation, Writing – review & editing. BL: Investigation, Writing – review & editing. AB: Formal analysis, Investigation, Writing – review & editing. RC: Investigation, Writing – review & editing. JG: Writing – review & editing, Conceptualization, Funding acquisition, Methodology, Project administration, Supervision, Visualization, Writing – original draft. AW: Conceptualization, Funding acquisition, Methodology, Project administration, Supervision, Visualization, Writing – original draft, Writing – review & editing.

## Funding

The author(s) declare that financial support was received for the research, authorship, and/or publication of this article. The work was funded in part by National Institutes of Health grants R21AI113736 (RP), R01AI123010 (AW), R01AI111899 (JG), R01AI140799 (JG), R01MH108179 (JG).

## Acknowledgments

We thank the current and past members of the UNC International Center for Translational Science (ICATS) for technical assistance. We also thank the technical staff at the UNC Biomedical Research Imaging Center, UNC Pathology Services Core, the Marsico Lung Institute Tissue and Procurement Core, and the Division of Comparative Medicine. We thank P. Collins and M. Peeples for generating the recombinant RSV expressing GFP and luciferase and B. Graham (NIAID) and A. Proria (Duke University) for the RSV-infected human lung tissues.

## Conflict of interest

The authors declare that the research was conducted in the absence of any commercial or financial relationships that could be construed as a potential conflict of interest.

The author(s) declared that they were an editorial board member of Frontiers, at the time of submission. This had no impact on the peer review process and the final decision.

## Publisher's note



## Supplementary material

The Supplementary Material for this article can be found online at: https://www.frontiersin.org/articles/10.3389/fviro.2024.1380030/full#supplementary-material

# References


1. Guo-Parke H, Canning P, Douglas I, Villenave R, Heaney LG, Coyle PV, et al. Relative respiratory syncytial virus cytopathogenesis in upper and lower respiratory tract epithelium. *Am J Respir Crit Care Med*. (2013) 188:842–51. doi: 10.1164/rccm.201304-0750OC

2. Shi T, McAllister DA, O'Brien KL, Simoes EAF, Madhi SA, Gessner BD, et al. Global, regional, and national disease burden estimates of acute lower respiratory infections due to respiratory syncytial virus in young children in 2015: a systematic review and modelling study. *Lancet*. (2017) 390:946–58. doi: 10.1016/S0140-6736(17)30938-8

3. Li Y, Wang X, Blau DM, Caballero MT, Feikin DR, Gill CJ, et al. Global, regional, and national disease burden estimates of acute lower respiratory infections due to respiratory syncytial virus in children younger than 5 years in 2019: a systematic analysis. *Lancet*. (2022) 399:2047–64. doi: 10.1016/S0140-6736(22)00478-0

4. Tseng HF, Sy LS, Ackerson B, Solano Z, Slezak J, Luo Y, et al. Severe morbidity and short- and mid- to long-term mortality in older adults hospitalized with respiratory syncytial virus infection. *J Infect Dis*. (2020) 222:1298–310. doi: 10.1093/infdis/jiaa361

5. Pilie P, Werbel WA, Jt R, Shu X, Schaubel D, Gregg KS. Adult patients with respiratory syncytial virus infection: impact of solid organ and hematopoietic stem cell transplantation on outcomes. *Transpl Infect Dis*. (2015) 17:551–7. doi: 10.1111/tid.12409

6. Robinson JL, Grenier D, MacLusky I, Allen UD. Respiratory syncytial virus infections in pediatric transplant recipients: A Canadian Paediatric Surveillance Program study. *Pediatr Transplant*. (2015) 19:659–62. doi: 10.1111/petr.12553

7. Shah JN, Chemaly RF. Management of RSV infections in adult recipients of hematopoietic stem cell transplantation. *Blood*. (2011) 117:2755–63. doi: 10.1182/blood-2010-08-263400

8. Abu-Raya B, Vineta Paramo M, Reicherz F, Lavoie PM. Why has the epidemiology of RSV changed during the COVID-19 pandemic? *EClinicalMedicine*. (2023) 61:102089. doi: 10.1016/j.eclinm.2023.102089

9. Tanne JH. US faces triple epidemic of flu, RSV, and covid. *BMJ*. (2022) 379:o2681. doi: 10.1136/bmj.o2681

10. Centers For Disease Control and Prevention. Vaccination Trends-Adults: Centers for Disease Control and Prevention (2023). Available online at: https://www.cdc.gov/respiratory-viruses/data-research/dashboard/vaccination-trends-adults.html#:~:text=The%20percent%20of%20the%20population%20reporting%20receipt%20of%20a%20flu,%25%20(15.9%2D18.1).

11. Griffiths C, Drews SJ, Marchant DJ. Respiratory syncytial virus: infection, detection, and new options for prevention and treatment. *Clin Microbiol Rev*. (2017) 30:277–319. doi: 10.1128/CMR.00010-16

12. Hayden FG, Whitley RJ. Respiratory syncytial virus antivirals: problems and progress. *J Infect Dis*. (2020) 222:1417–21. doi: 10.1093/infdis/jiaa029

13. Hegele RG. Respiratory syncytial virus therapy and prophylaxis: have we finally turned the corner? *Eur Respir J*. (2011) 38:246–7. doi: 10.1183/09031936.00012011

14. Griffin MP, Yuan Y, Takas T, Domachowske JB, Madhi SA, Manzoni P, et al. Single-dose nirsevimab for prevention of RSV in preterm infants. *N Engl J Med*. (2020) 383:415–25. doi: 10.1056/NEJMoa1913556

15. Domachowske JB, Anderson EJ, Goldstein M. The future of respiratory syncytial virus disease prevention and treatment. *Infect Dis Ther*. (2021) 10:47–60. doi: 10.1007/s40121-020-00383-6

16. Welliver TP, Garofalo RP, Hosakote Y, Hintz KH, Avendano L, Sanchez K, et al. Severe human lower respiratory tract illness caused by respiratory syncytial virus and influenza virus is characterized by the absence of pulmonary cytotoxic lymphocyte responses. *J Infect Dis*. (2007) 195:1126–36. doi: 10.1086/512615

17. Pickles RJ, DeVincenzo JP. Respiratory syncytial virus (RSV) and its propensity for causing bronchiolitis. *J Pathol*. (2015) 235:266–76. doi: 10.1002/path.4462

18. Wahl A, De C, Abad Fernandez M, Lenarcic EM, Xu Y, Cockrell AS, et al. Precision mouse models with expanded tropism for human pathogens. *Nat Biotechnol*. (2019) 37:1163–73. doi: 10.1038/s41587-019-0225-9

19. Wahl A, Gralinski LE, Johnson CE, Yao W, Kovarova M, Dinnon KH 3rd, et al. SARS-CoV-2 infection is effectively treated and prevented by EIDD-2801. *Nature*. (2021) 591:451–7. doi: 10.1038/s41586-021-03312-w

20. De C, Pickles RJ, Yao W, Liao B, Boone A, Choi M, et al. Human T cells efficiently control RSV infection. *JCI Insight*. (2023) 8. doi: 10.1172/jci.insight.168110

21. Hallak LK, Spillmann D, Collins PL, Peeples ME. Glycosaminoglycan sulfation requirements for respiratory syncytial virus infection. *J Virol*. (2000) 74:10508–13. doi: 10.1128/JVI.74.22.10508-10513.2000

22. Johnson JE, Gonzales RA, Olson SJ, Wright PF, Graham BS. The histopathology of fatal untreated human respiratory syncytial virus infection. *Mod Pathol*. (2007) 20:108–19. doi: 10.1038/modpathol.3800725

23. Talukdar SN, Osan J, Ryan K, Grove B, Perley D, Kumar BD, et al. RSV-induced expanded ciliated cells contribute to bronchial wall thickening. *Virus Res*. (2023) 327:199060. doi: 10.1016/j.virusres.2023.199060

24. Okuda K, Chen G, Subramani DB, Wolf M, Gilmore RC, Kato T, et al. Localization of secretory mucins MUC5AC and MUC5B in normal/healthy human airways. *Am J Respir Crit Care Med*. (2019) 199:715–27. doi: 10.1164/rccm.201804-0734OC

25. Hill DB, Button B, Rubinstein M, Boucher RC. Physiology and pathophysiology of human airway mucus. *Physiol Rev*. (2022) 102:1757–836. doi: 10.1152/physrev.00004.2021

26. Harford TJ, Rezaee F, Dye BR, Fan J, Spence JR, Piedimonte G. RSV-induced changes in a 3-dimensional organoid model of human fetal lungs. *PloS One*. (2022) 17:e0265094. doi: 10.1371/journal.pone.0265094

27. Stokes KL, Chi MH, Sakamoto K, Newcomb DC, Currier MG, Huckabee MM, et al. Differential pathogenesis of respiratory syncytial virus clinical isolates in BALB/c mice. *J Virol*. (2011) 85:5782–93. doi: 10.1128/JVI.01693-10

28. Moore ML, Chi MH, Luongo C, Lukacs NW, Polosukhin VV, Huckabee MM, et al. A chimeric A2 strain of respiratory syncytial virus (RSV) with the fusion protein of RSV strain line 19 exhibits enhanced viral load, mucus, and airway dysfunction. *J Virol*. (2009) 83:4185–94. doi: 10.1128/JVI.01853-08

29. Boyoglu-Barnum S, Gaston KA, Todd SO, Boyoglu C, Chirkova T, Barnum TR, et al. A respiratory syncytial virus (RSV) anti-G protein F(ab')2 monoclonal antibody suppresses mucous production and breathing effort in RSV rA2-line19F-infected BALB/c mice. *J Virol*. (2013) 87:10955–67. doi: 10.1128/JVI.01164-13

30. Hashimoto K, Durbin JE, Zhou W, Collins RD, Ho SB, Kolls JK, et al. Respiratory syncytial virus infection in the absence of STAT 1 results in airway dysfunction, airway mucus, and augmented IL-17 levels. *J Allergy Clin Immunol*. (2005) 116:550–7. doi: 10.1016/j.jaci.2005.03.051

31. Everard ML, Swarbrick A, Wrightham M, McIntyre J, Dunkley C, James PD, et al. Analysis of cells obtained by bronchial lavage of infants with respiratory syncytial virus infection. *Arch Dis Child*. (1994) 71:428–32. doi: 10.1136/adc.71.5.428

32. Geerdink RJ, Pillay J, Meyaard L, Bont L. Neutrophils in respiratory syncytial virus infection: A target for asthma prevention. *J Allergy Clin Immunol*. (2015) 136:838–47. doi: 10.1016/j.jaci.2015.06.034

33. McNamara PS, Ritson P, Selby A, Hart CA, Smyth RL. Bronchoalveolar lavage cellularity in infants with severe respiratory syncytial virus bronchiolitis. *Arch Dis Child*. (2003) 88:922–6. doi: 10.1136/adc.88.10.922

34. Liesman RM, Buchholz UJ, Luongo CL, Yang L, Proia AD, DeVincenzo JP, et al. RSV-encoded NS2 promotes epithelial cell shedding and distal airway obstruction. *J Clin Invest*. (2014) 124:2219–33. doi: 10.1172/JCI72948

35. Rezaee F, DeSando SA, Ivanov AI, Chapman TJ, Knowlden SA, Beck LA, et al. Sustained protein kinase D activation mediates respiratory syncytial virus-induced airway barrier disruption. *J Virol*. (2013) 87:11088–95. doi: 10.1128/JVI.01573-13

36. Linfield DT, Gao N, Raduka A, Harford TJ, Piedimonte G, Rezaee F. RSV attenuates epithelial cell restitution by inhibiting actin cytoskeleton-dependent cell migration. *Am J Physiol Lung Cell Mol Physiol*. (2021) 321:L189–203. doi: 10.1152/ajplung.00118.2021

37. Zhang Y, Wang Y, Zhao J, Xiong Z, Fan Y, Zhang W, et al. Severity and mortality of respiratory syncytial virus vs influenza A infection in hospitalized adults in China. *Influenza Other Respir Viruses*. (2020) 14:483–90. doi: 10.1111/irv.12754

38. Bourzac K. Respiratory syncytial virus co-infections might conspire to worsen disease. *Nature*. (2023) 621:S60–S1. doi: 10.1038/d41586-023-02959-x

39. Li Y, Pillai P, Miyake F, Nair H. The role of viral co-infections in the severity of acute respiratory infections among children infected with respiratory syncytial virus (RSV): A systematic review and meta-analysis. *J Glob Health*. (2020) 10:010426. doi: 10.7189/jogh.10.010426